Electronic Supplementary Information (ESI)

Green cellulose nanofiber-based printed electrode for practical highly sensitive amoxicillin detection

Shaimah Rinda Sari,[a] Erika Shinchi,[b] Kenji Shida,[c] Yuly Kusumawati,[d] Kartika A. Madurani,[e] Fredy Kurniawan[e] and Masato Tominaga*[a]

[a] Graduate School of Science and Engineering, Saga University, 1 Honjomachi, Saga 840-8502, Japan

[b] Analytical Research Center for Experimental Sciences, Saga University, 1 Honjomachi, Saga 840-8502, Japan

[c] Faculty of Engineering, Kumamoto University, 2-39-1 Kurokami, Kumamoto 860-8555, Japan

[d] Chemistry Department, Faculty of Sciences and Data Analytics, Institut Teknologi Sepuluh Nopember, Surabaya 60111, Indonesia

[e] Laboratory of Instrumentation and Analytical Sciences, Chemistry Department, Faculty of Science and Data Analytics, Institut Teknologi Sepuluh Nopember, Surabaya 60111, Indonesia

*Corresponding author, Email: masato@cc.saga-u.ac.jp

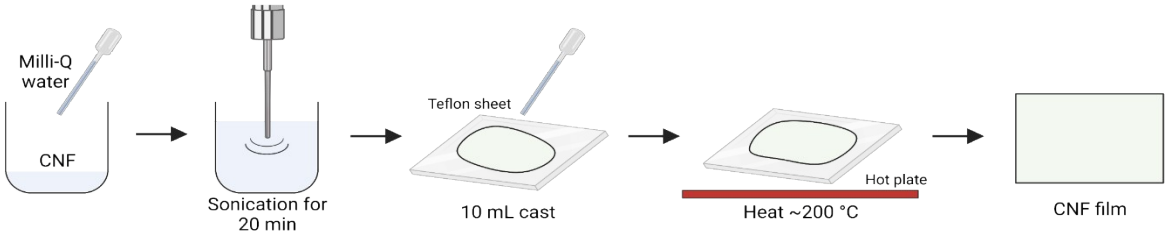

Fig. S1 Scheme of CNF film preparation.

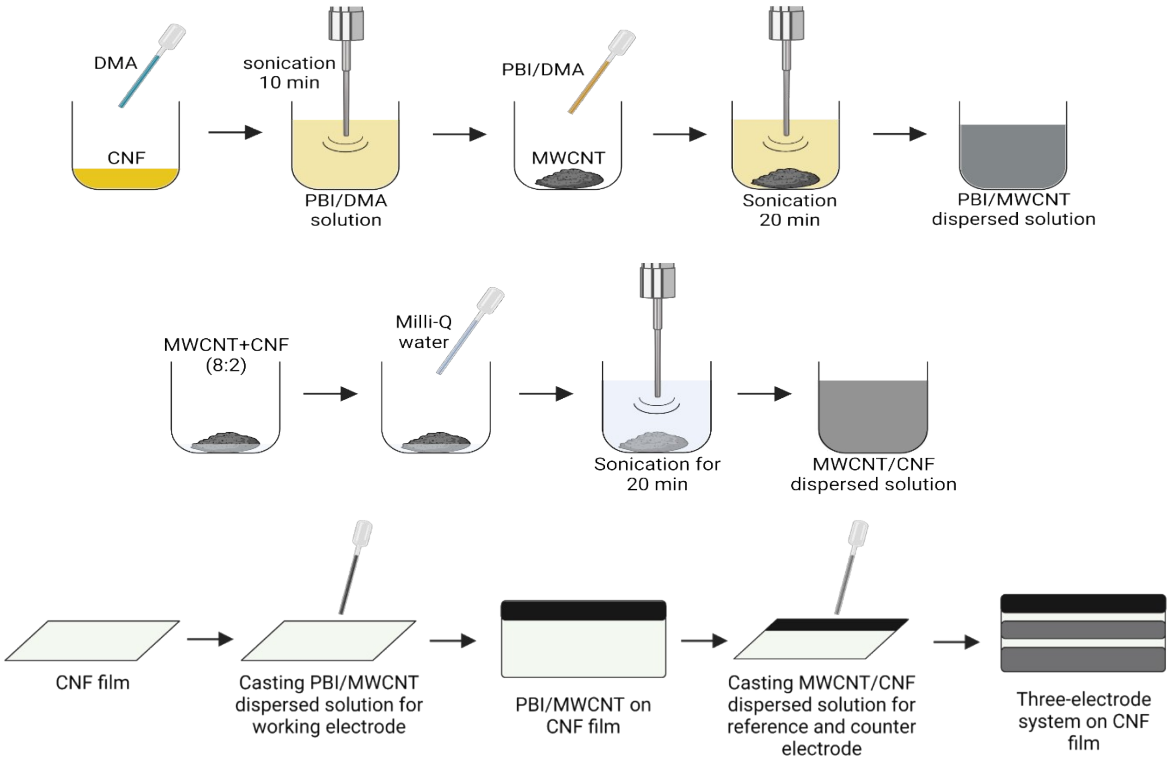

Fig. S2 Scheme of CNF-based printed electrode preparation.

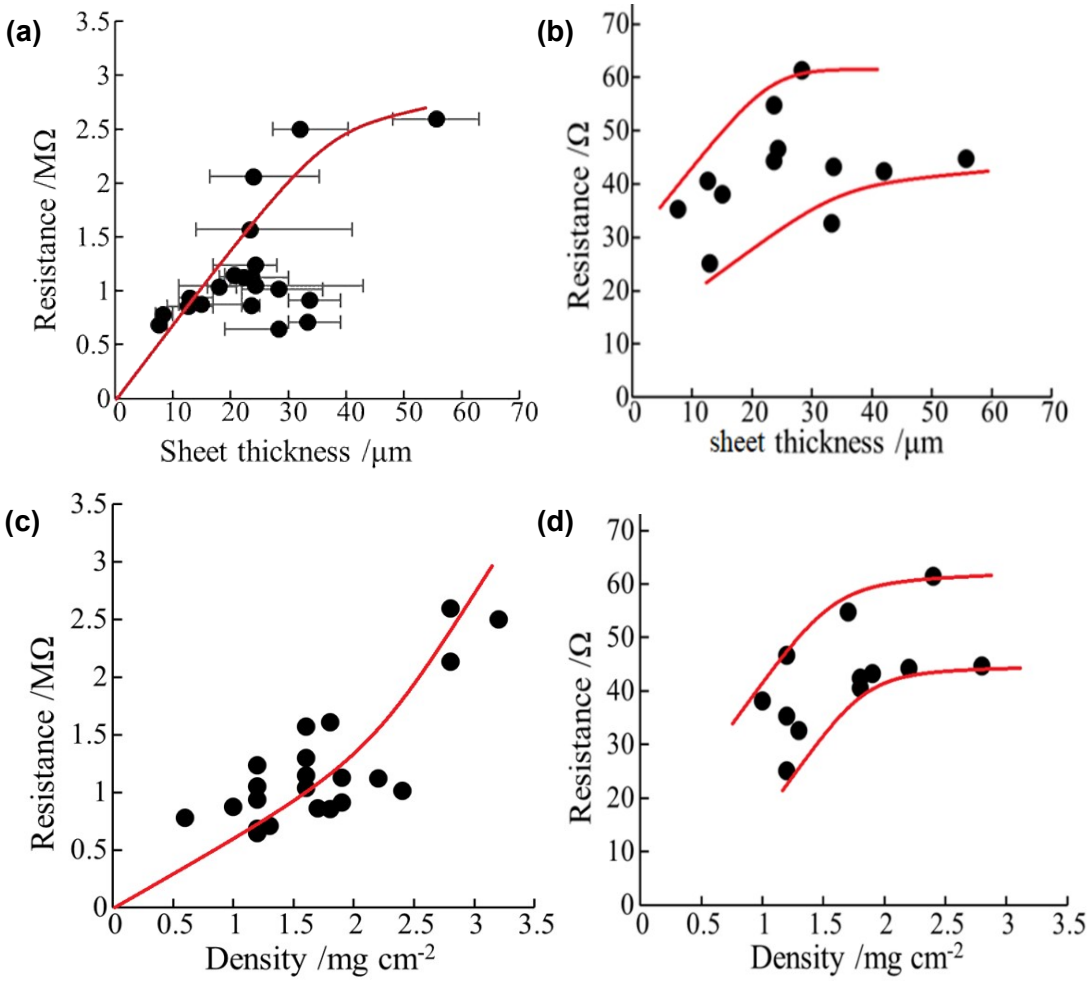

Fig. S3 The variation of the resistance number as a function of the CNF film thickness for dry condition (a) and wet condition containing 0.1 M Na_2SO_4 pH 7 (b). Resistivity vs. density for CNF film in dry condition (c) and wet condition containing 0.1 M Na_2SO_4 pH 7 (d).

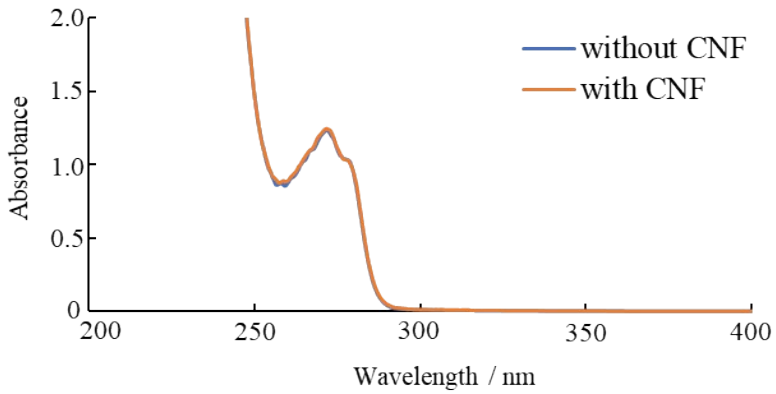

Fig. S4 Ultraviolet-visible spectroscopy of 0.1 M Na_2SO_4 (pH 7) solution containing 100 µM AMX in the absence (blue line) and presence (orange line) of CNF film with 1 hour immersion time.

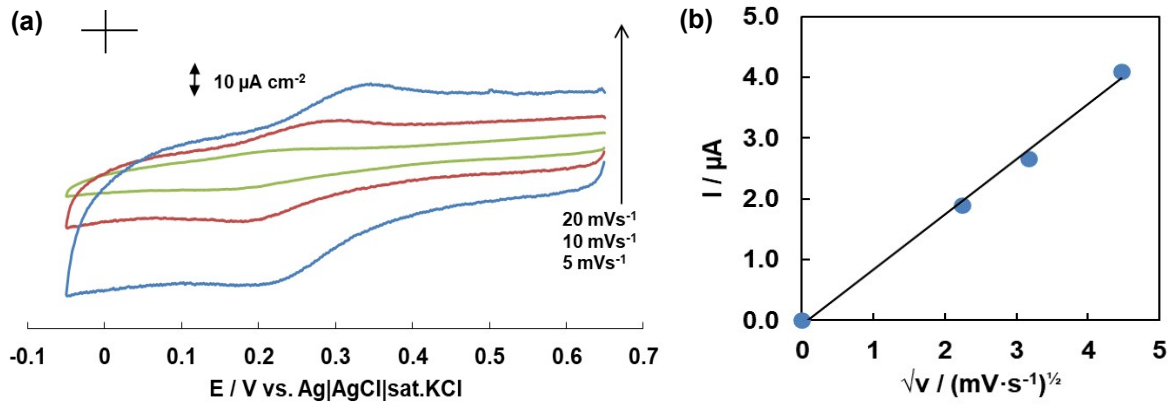

Fig. S5 Cyclic voltammograms of 1.0 mM $[Fe(CN)_6]^{3-}$ at the PBI/MWCNT-modified CNF-based printed electrode in 1.0 M KCl solution (pH 7) at various potential sweep rates (a) and plot of the cathodic peak current *versus* the square root of the potential sweep rate (b). UV-ozone treatment was performed for 3 min prior to each electrochemical measurements for the printed electrode.

CNF showed a typical cellulose I crystal form with characteristic peaks around 2θ = 16.5° and 22.5° which corresponds to the (010) and (110), respectively. While the characteristic peak around 2θ = 26° corresponds to the C (002) was not prominent thought to be the result of it merging with broad CNF peaks. With the addition of polymer matrix such as PBI, intensity of the characteristic peaks (CNF and MWCNT) was decreased, which indicated that amorphous PBI wrapped around the CNT nanofibers and on the surface of CNF. While all the diffraction peak intensities decreased in the nanocomposite, both the original characteristic structure of cellulose and carbon nanotube were still observed in the composite, suggesting a well-incorporation between the hybrid components.[1]

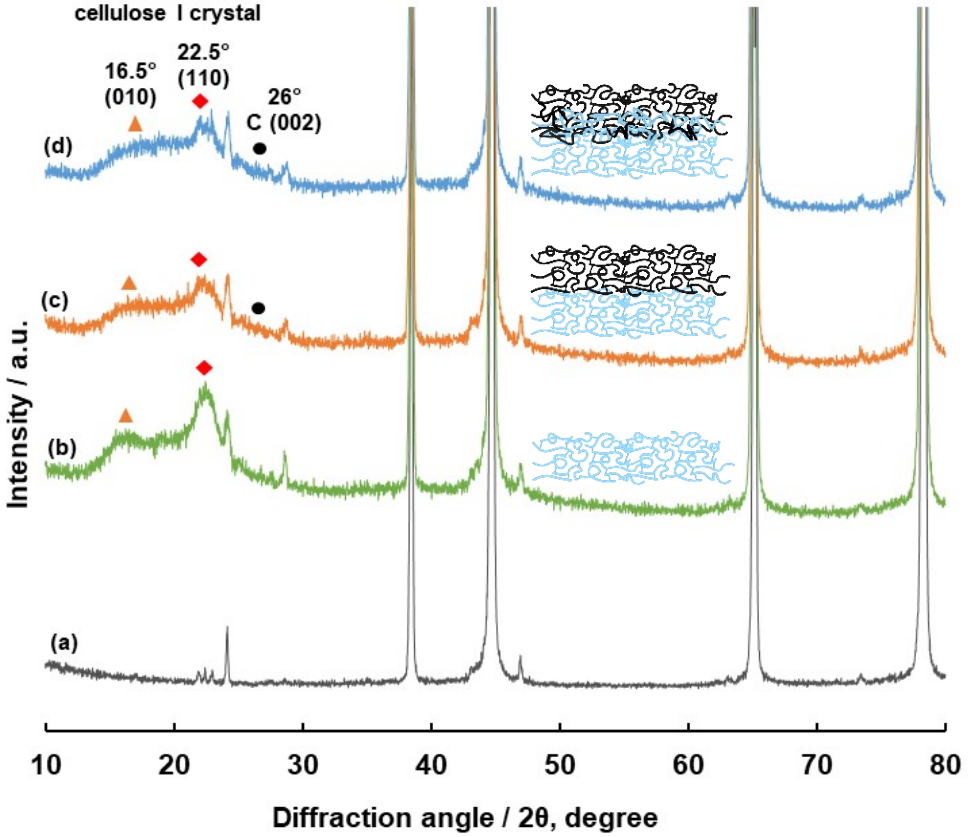

Fig. S6 XRD patterns of aluminium plate (a), CNF film (b), MWCNT/CNF (c) and PBI/MWCNT/CNF (d).

Figure S7 shows a characteristic band assigned to –OH stretching of intramolecular hydrogen bonds in CNF[2] was observed at 3400 cm^{-1}. For both PBI/MWCNT/CNF samples in absence or presence of AMX, the intensities of the bands assigned to vibrations of C–H (2900 cm^{-1}), –CH2 (1430 and 896 cm^{-1}), and C–H (1373 and 896 cm^{-1}) were much smaller or absent proving CNF film was covered with layers of PBI/MWCNT. PBI characteristic bands appeared around 1610 and 802 cm^{-1} were also observed for both PBI/MWCNT/CNF samples. Special for PBI/MWCNT/CNF sample with AMX, peaks assigned for C=O stretching vibration of carbonyl group (1735 cm^{-1}), C-H bending vibration (1247 cm^{-1}), and benzene ring bending vibration (844 cm^{-1}) were observed proving successful interaction between the modified film with AMX.

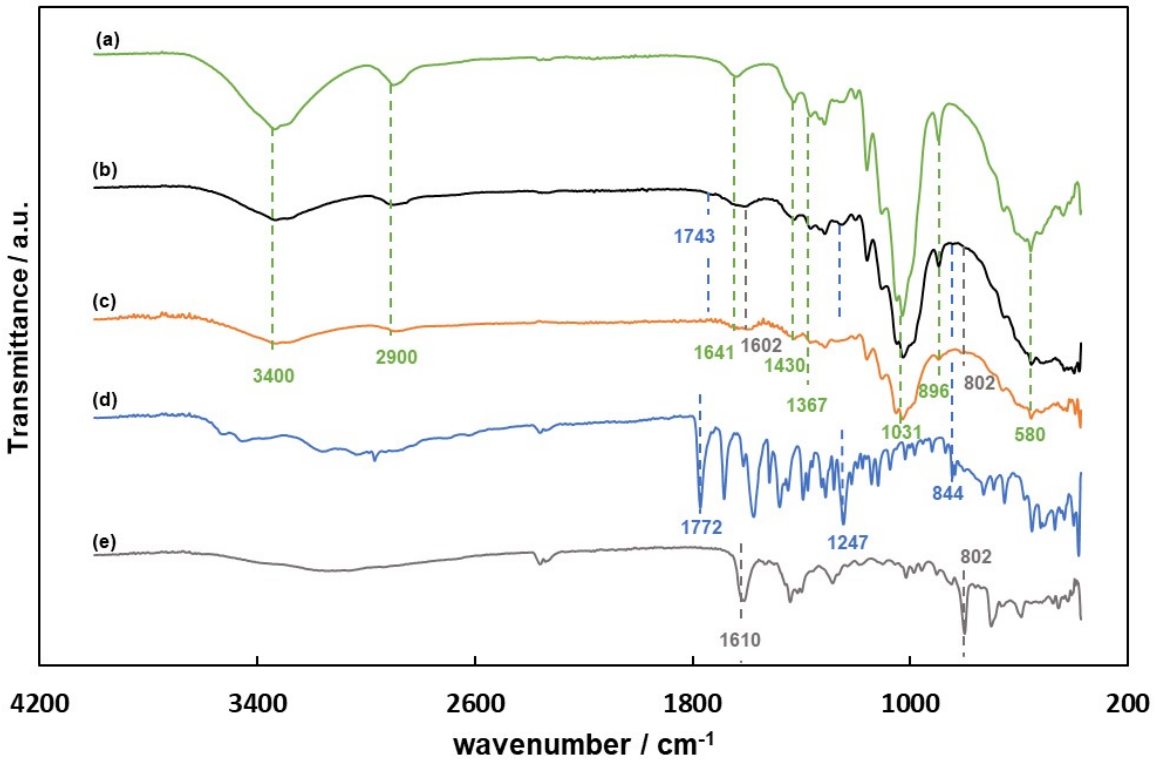

Fig. S7 FT-IR spectra of CNF (a), PBI/MWCNT/CNF with AMX (b), PBI/MWCNT/CNF without AMX (c), AMX (d), and PBI (e).

Computational simulation

Adsorption configuration was carefully designed and optimized by analyzing the possible binding sites in amoxicillin molecules. The interactions between the adsorbing amoxicillin molecule and benzimidazole molecule in the electrode surface were performed using the B3LYP level[3] with 6-31G* basis sets[4,5] implemented in the Gaussian 16 code.[6] Avogadro 1.2.0 was used to visualize the calculation results including energy of the highest occupied molecular orbital (E_{HOMO}), lowest unoccupied molecular orbital energy (E_{LUMO}) and Mulliken charges. The E_{ads} (adsorption energy) were obtained as follows[7,8]

$$E_{ads} = E_{amoxicillin+benzimidazole} - \left(E_{amoxicillin} + E_{benzimidazole}\right) \quad (1)$$

where $E_{amoxicillin+benzimidazole}$ represent the total energies of the interacted amoxicillin-benzimidazole in optimized adsorption configuration. Whereas $E_{amoxicillin}$ and $E_{benzimidazole}$ are isolated amoxicillin and benzimidazole molecule, respectively. The E_{ads} calculation shows the stability of amoxicillin-benzimidazole interactions on the electrode surface.[9,10]

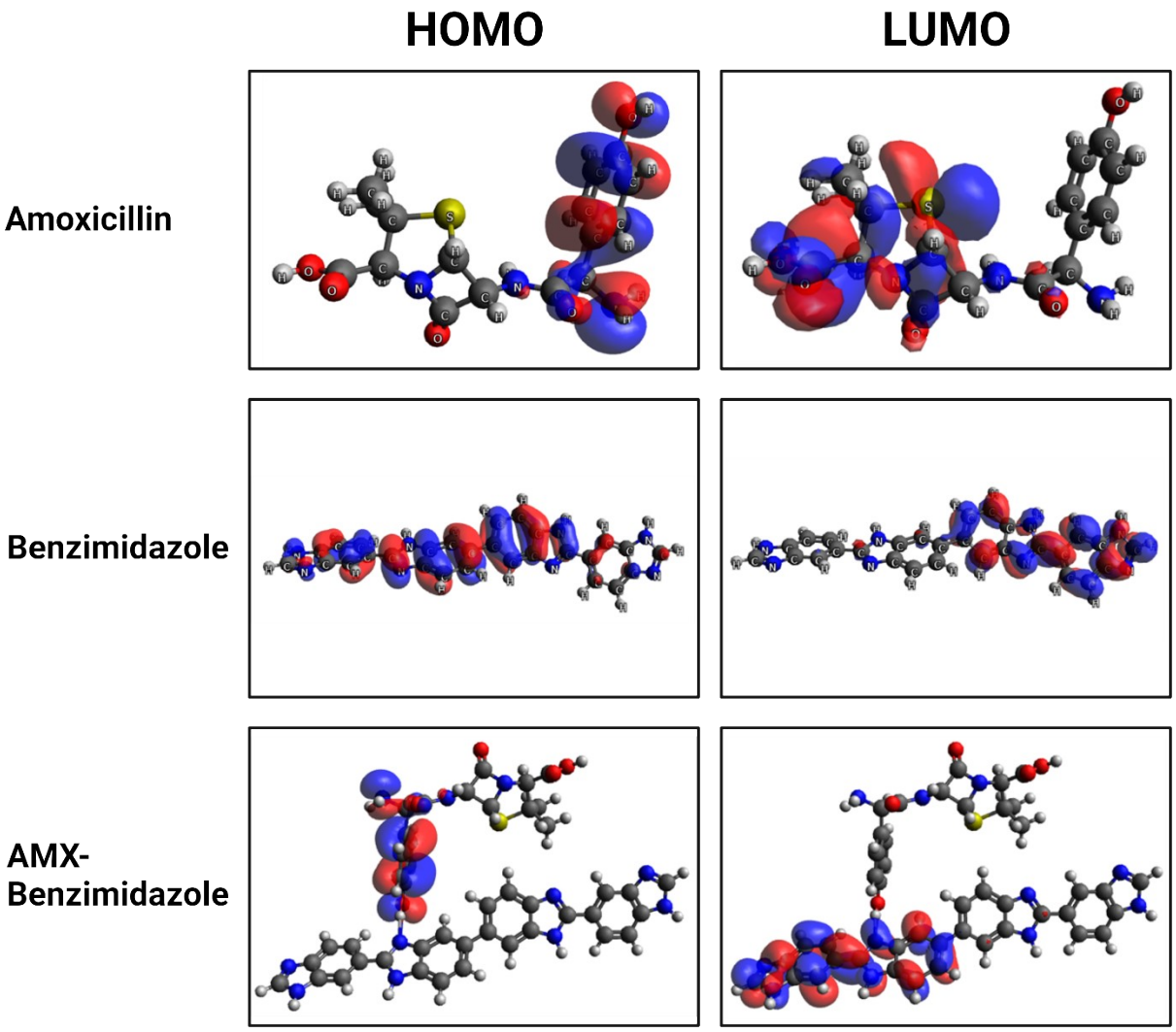

Fig. S8 Distribution of highest occupied molecular orbital (HOMO) and lowest unoccupied molecular orbital (LUMO) for AMX with benzimidazole from computational simulation GAMESS. Color illustration: positive electrostatic potential is shown in dark blue and negative in red.

Table S1 The calculated adsorption energy (E_{ads}), binding distance (d) and charge transfer (Q) for possible amoxicillin molecule adsorption over benzimidazole surface.

System	E_{ads} (kJ/mol)	$d_{(O)\text{-}PBI}$ (Å)	Q_{AMX}	Q_{PBI}
AMX-Benzimidazole	–57.05	2.812	-0.063	0.063

Table S2 Reproducibility of reference electrode using CNF-based printed electrode.

Reference electrode	***E* / V vs. Ag|AgCl|sat.KCl**
A	0.61
B	0.62
C	0.61
D	0.60
E	0.59
F	0.61
G	0.61
H	0.62
I	0.59

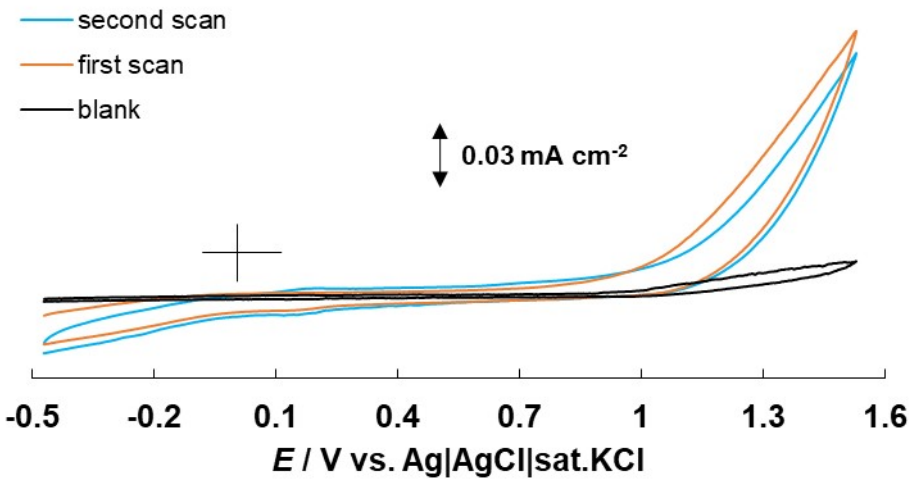

Fig. S9 CV recorded at the PBI/MWCNT-modified CNF-based printed electrode in 0.1 M Na_2SO_4 pH 7 for blank, first scan and second scan in the presence of 100 µM AMX. Potential sweep rate: 10 mV s^{-1}.

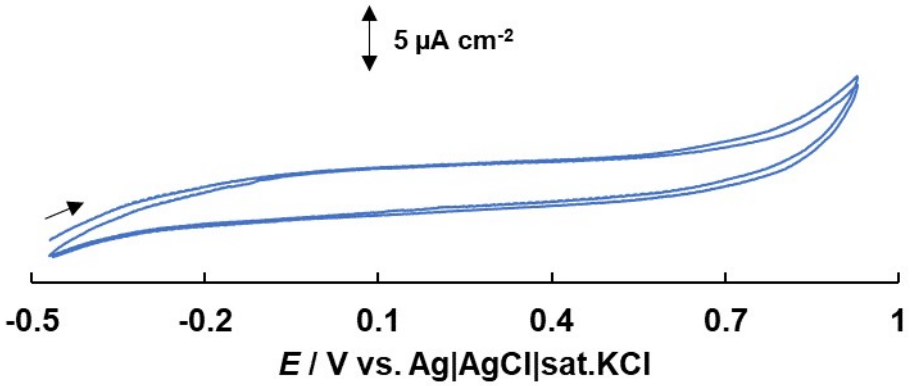

Fig. S10 CV recorded for shorter potential range at the PBI/MWCNT-modified CNF-based printed electrode in 0.1 M Na_2SO_4 pH 7 containing 100 µM AMX. Potential sweep rate: 10 mV s^{-1}.

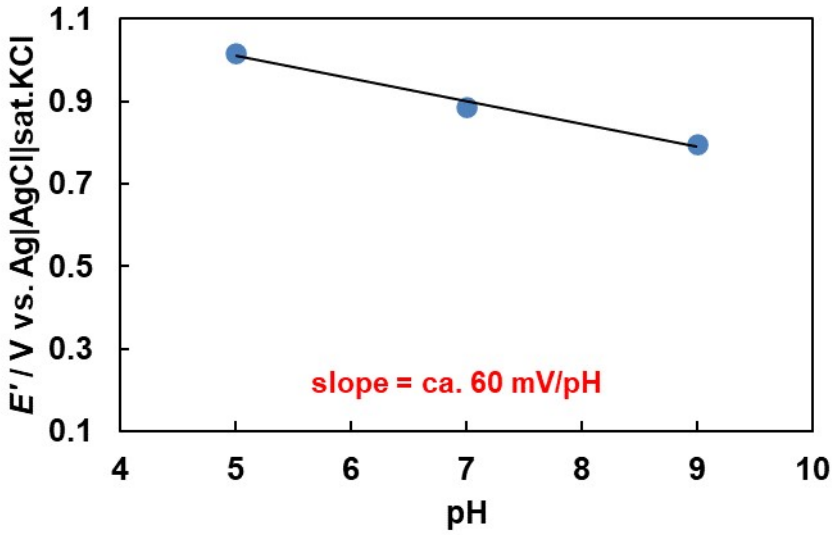

Fig. S11 Plots of offset potentials vs. pH for first oxidation reaction at ca. 0.9 V in 0.1 M Na_2SO_4 solution (pH 7) containing 100 µM AMX using the PBI/MWCNT-modified CNF-based printed electrode.

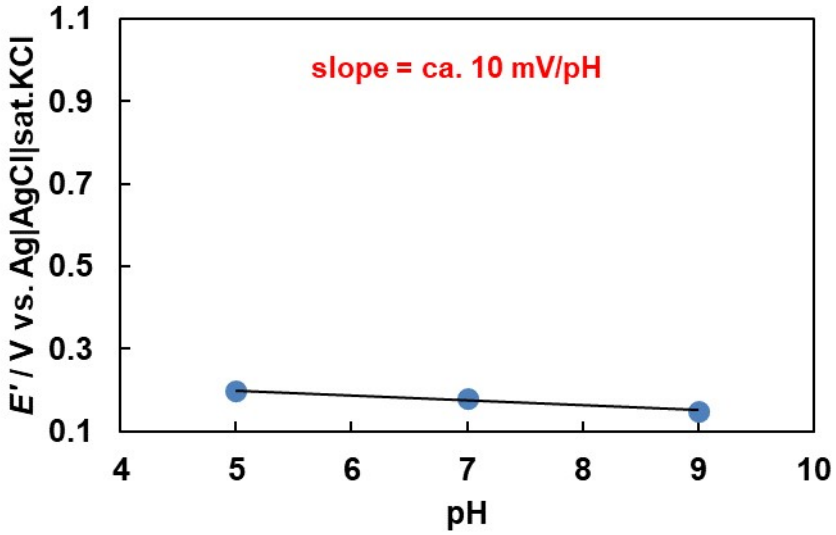

Fig. S12 Plots of offset potentials vs. pH for second oxidation reaction at ca. 0.18 V in 0.1 M Na_2SO_4 solution (pH 7) containing 100 µM AMX using the PBI/MWCNT-modified CNF-based printed electrode.

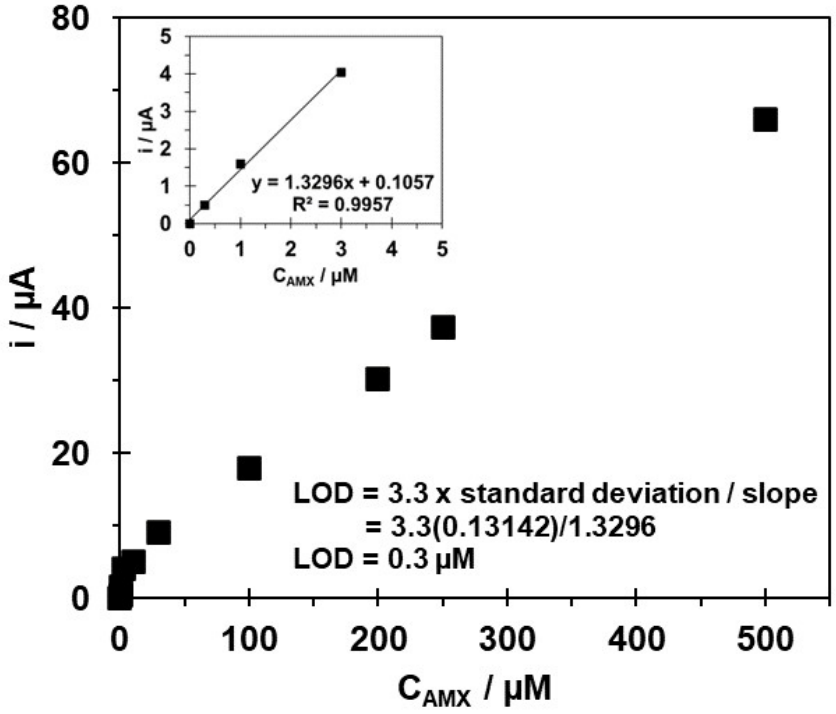

Fig. S13 Estimation of limit of detection (LOD) for AMX determination using CNF-based printed electrode. LOD was estimated from the standard deviation of the response (σ) of the curve and the slope of the calibration curve (S) at linear part of the calibration curve as shown on the inset approximating the LOD according to the formula: LOD = 3.3(σ/S), represented in the figure.

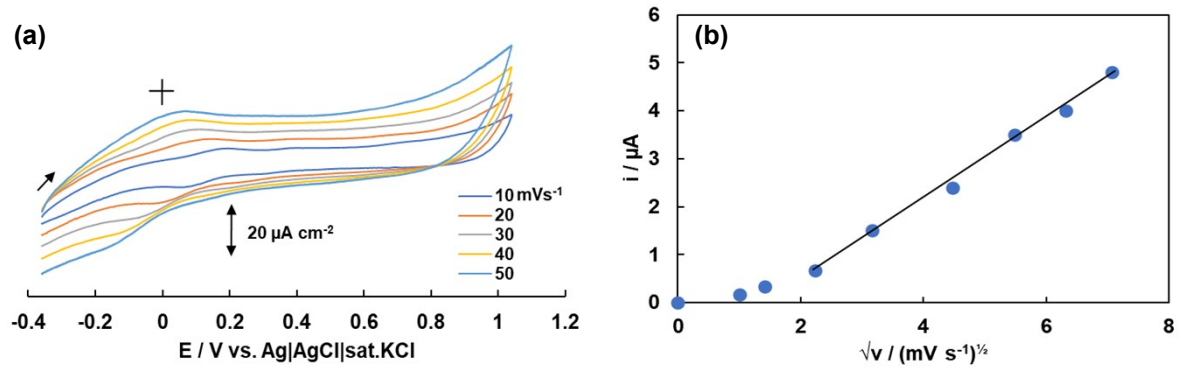

Fig. S14 Cyclic voltammograms of 30 µM AMX at the PBI/MWCNT-modified CNF-based printed electrode in 0.1 M Na_2SO_4 solution (pH 7) at various potential sweep rates (a) and plot of the cathodic peak current *versus* the square root of potential sweep rate (b).

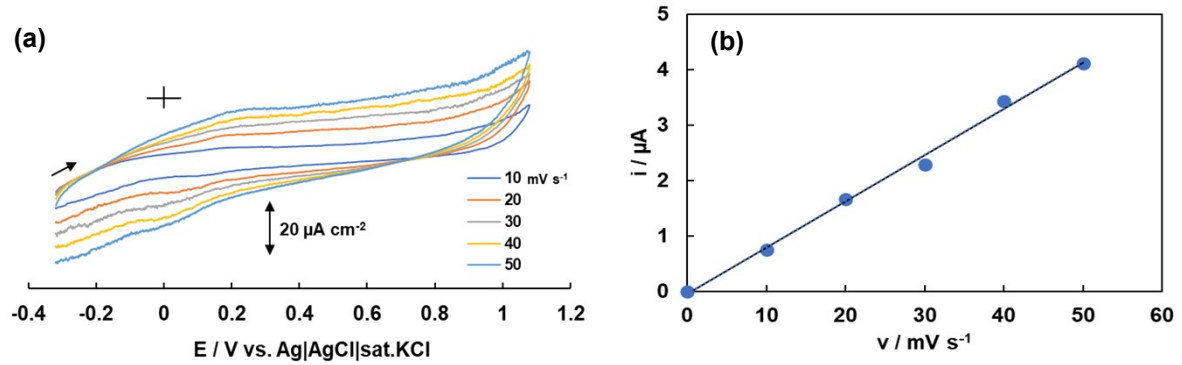

Fig. S15 Cyclic voltammograms of 1.0 µM AMX at the PBI/MWCNT-modified CNF-based printed electrode in 0.1 M Na_2SO_4 solution (pH 7) at various potential sweep rates (a) and plot of the cathodic peak current *versus* the potential sweep rate (b).

Randles-Sevcik equation

$$i_p = \pm \left(2.69 \times 10^5\right) n^{3/2} A D^{1/2} C v^{1/2} \quad (2)$$

where,

i_p : cathodic peak current (A cm^{-2})
n : number of electrons involved in the reaction; assuming n = 1
A : electrode surface area (A = 1 cm^{-2})
D : diffusion coefficient (cm^2 s^{-1})
C : redox probe concentration (C = 3×10^{-5} mol cm^{-3})
v : potential scan rate (V s^{-1})

Nicholson equation

$$\Psi = k_s[\pi DnvF/(RT)]^{-1/2} \quad (3)$$

where,

Ψ	:	kinetic parameter
k_s	:	electron transfer rate constant (cm s^{-1})
F	:	Faraday's constant (96485C mol^{-1})
RT	:	Boltzmann constant; R = 8.314 J K mol^{-1}, T ≈ 298.15 K

Adsorption isotherm

For an ideal electrochemical reaction involving a surface-bound species, considering the rate equation for a totally irreversible one-step, one-electron reaction,[11] can be written as

$$i = FAk^o C_O^{*(1-\alpha)} C_R^{*\alpha} \quad (4)$$

where,

i	:	cathodic peak current (A cm^{-2})
k^o	:	standard rate constant at the surface
F	:	Faraday's constant (96485C mol^{-1})
A	:	electrode surface area (A = 1 cm^{-2})
C_O	:	initial concentration of O (1×10^{-6} mol cm^{-3})
C_R	:	initial concentration of R (1×10^{-6} mol cm^{-3})
α	:	transfer coefficient (α = 0.5)

Stokes-Einstein equation

$$D = RT/6\pi r\eta N \quad (5)$$

where,

D	:	diffusion coefficient (cm^2 s^{-1})
r	:	radius of amoxicillin molecule (cm)
η	:	viscosity of solvent (P)
		η_{25} of pure water = 0.00895 poise
N	:	Avogadro's number
R	:	gas constant (erg K^{-1} mol^{-1})
T	:	temperature (K)

$$D_1 = \frac{(8.314 \times 10^7)(298)}{6\pi(7.25 \times 10^{-8})(0.00895)(1)} = 6.75 \times 10^{-6} cm^{-2} s^{-1}$$

$$D_2 = \frac{(8.314 \times 10^7)(298)}{6\pi(9.30 \times 10^{-8})(0.00895)(1)} = 5.26 \times 10^{-6} cm^{-2} s^{-1}$$

$$D_3 = \frac{(8.314 \times 10^7)(298)}{6\pi(4.23 \times 10^{-8})(0.00895)(1)} = 1.16 \times 10^{-5} cm^{-2} s^{-1}$$

Electrochemically active surface area evaluated from double-layer capacitance

The electrochemically active surface area (ECSA) of a catalyst sample can be calculated with a cyclic voltammetry (CV) method. We calculated the double-layer capacitance (C_{dl}) of the PBI/MWCNT-modified CNF-based printed electrode based on the scan rate dependence of cyclic voltammetry measurements. By plotting the difference in current density between anodic and cathodic sweeps at a fixed potential (0.5 V vs Ag|AgCl|sat.KCl) against the scan rate, a linear trend is observed. The fitting slope is twice of C_{dl}, which is linearly proportional to the ECSA, according to the following formula:

$$ECSA = \frac{C_{dl}}{C_s} \tag{6}$$

where C_s is the specific capacitance. As seen from Fig. S14, for the PBI/MWCNT-modified CNF-based printed electrode, C_{dl} = 0.53 µF cm^{-2}. Assumed the C_s of the well-ordered graphite structure from our previously reported value of 2–5 µF cm^{-2} with small defect, the ECSA of 0.265–0.106 cm^2 was obtained.[12]

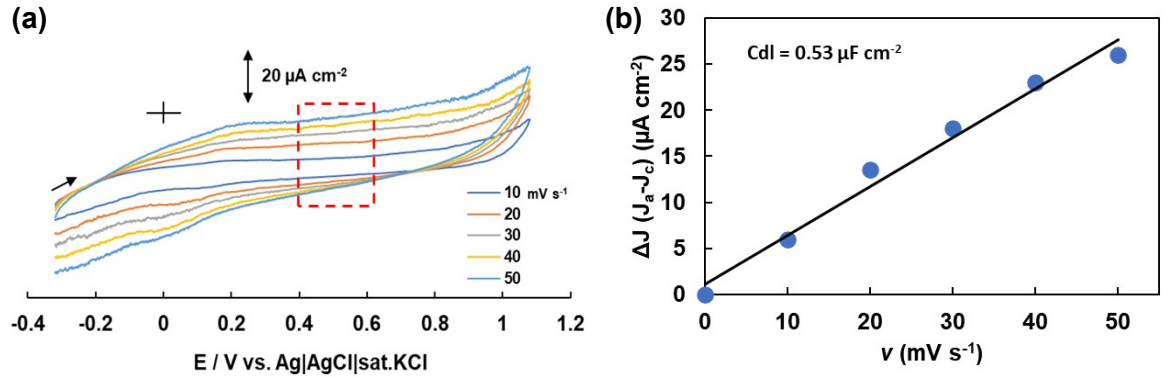

Fig. S16 (a) CV curves of the PBI/MWCNT-modified CNF-based printed electrode in 0.1 M Na_2SO_4 solution (pH 7) at different scan rate (10–50 mV s^{-1}) where potential window of non-Faradaic region from around 0.4 to 0.6 V was selected to determine C_{dl} (electrochemical double layer capacitance) and (b) Linear fitting of the current densities at 0.5 V versus scan rates for the previous CV measurements.

Theoretically surface concentration

- **Based on AMX molecule size**

$$\Gamma_{AMX} = \frac{\left[\frac{1\ moles}{(A\ (cm^{-2}))}\right]}{Avogadro's\ number} = \frac{[1/(2(137.4315)\times 10^{-16})cm^{-2}]}{6.022\times 10^{23}} = 6\times 10^{-11} mol\ cm^{-2}$$

- **Based on MWCNT specific surface area**

Specific surface area of MWCNT = 713 m^2 g^{-1}

M_w of AMX = ~400 g mol^{-1}

40 mg of MWCNT = 4×10^{-4} mol g^{-1}

$$\Gamma_{AMX} = \frac{4 \times 10^{-4}\ mol\ g^{-1}}{713\ m^2 g^{-1}} = \frac{4 \times 10^{-4}\ mol}{7.13 \times 10^{6}\ cm^2} = \sim 6\ \times 10^{-11}\ mol\ cm^{-2}$$

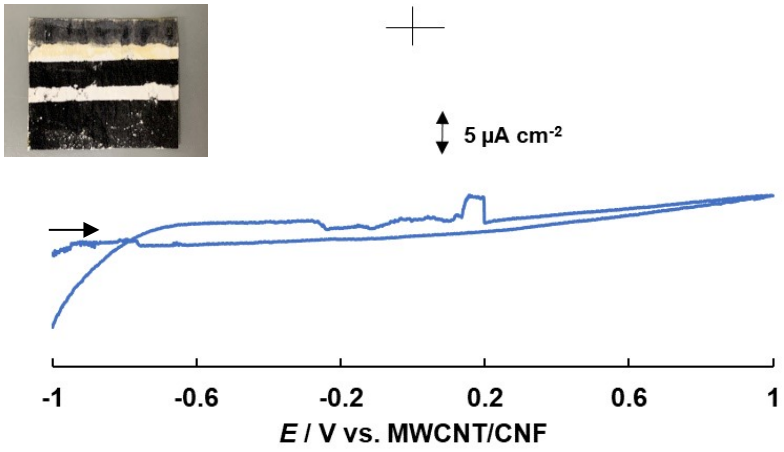

Fig. S17 Cyclic voltammograms recorded at 10 mv s^{-1} for the PBI/MWCNT-modified CNF-based printed electrode with copy paper platform in 0.1 M Na_2SO_4 pH 7 containing 100 µM AMX. The inset figure shows the modified disposable electrode.

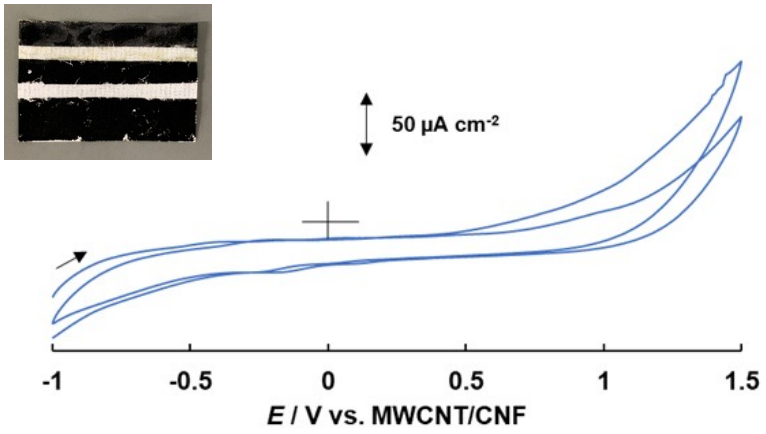

Fig. S18 Cyclic voltammograms recorded at 10 mv s^{-1} for the PBI/MWCNT-modified CNF-based printed electrode with calligraphy paper platform in 0.1 M Na_2SO_4 pH 7 containing 250 µM AMX. The inset figure shows the modified disposable electrode.

Table S3 Characteristics of different platform used for modified electrode.

Platform material	**Resistance / Ω**	**Average thickness / µm**	**Peak current / µA**	**Additional information**
CNF	120	39 ± 1	4	easy to modify
Copy paper	840	145 ± 1	not detected	difficult to modify within template

Calligraphy paper	390	80 ± 1	2.5	difficult to modify within template, poor sensitivity

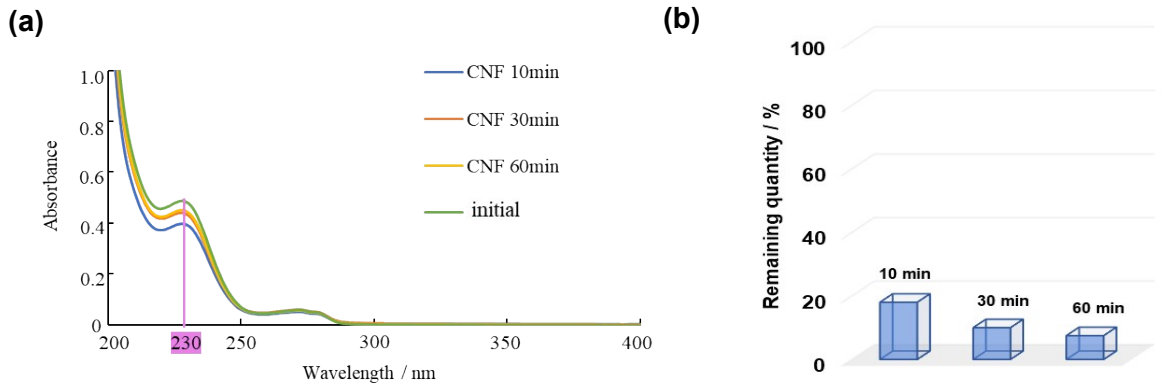

Fig. S19 Ultraviolet-visible spectroscopy of amoxicillin adsorption behavior on CNF film (a) and remaining amount of amoxicillin on CNF film with different immersion time inside 0.1 M Na_2SO_4 solution (pH 7) (b). At first, CNF films were treated with 100 µM AMX solution and left to dry overnight under vacuum conditions (0.06 MPa). They were then immersed in 0.1 M Na_2SO_4 solution (pH 7) for 10, 30, and 60 minutes prior to measurements.

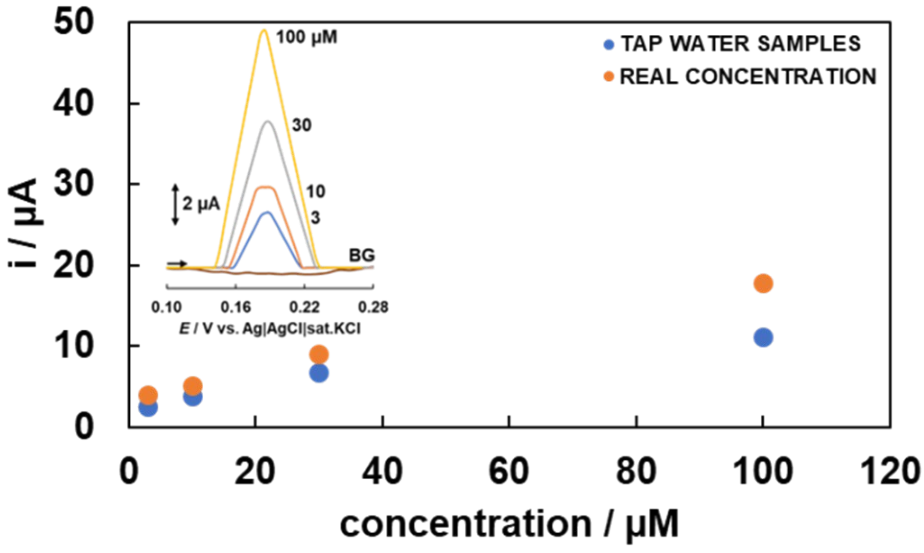

Fig. S20 AMX concentrations versus peak current value comparison for real concentration and tap water samples. Insets show the square wave voltammograms of the PBI/MWCNT-modified CNF-based printed electrode for tap water samples containing different concentration of AMX with supporting electrolyte of 0.1 M Na_2SO_4 solution (pH 7).

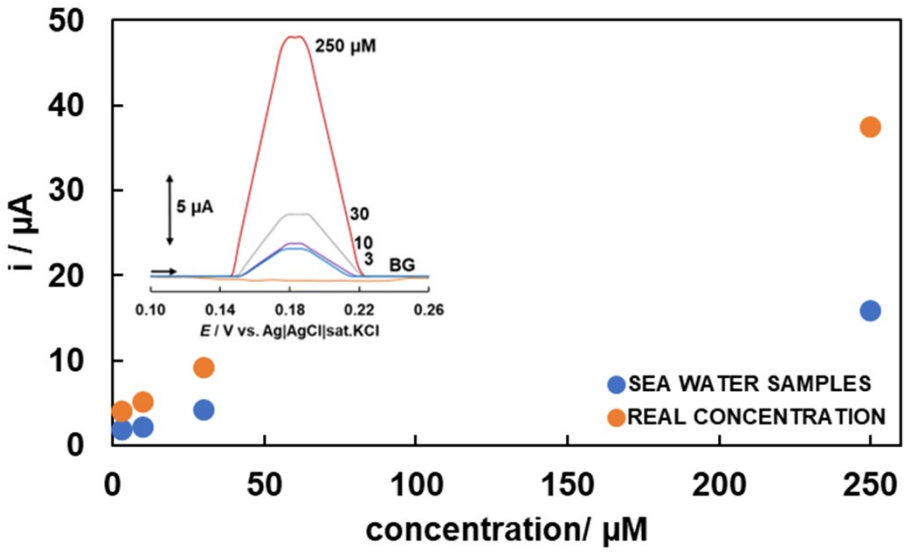

Fig. S21 AMX concentrations versus peak current value comparison for real concentration and sea water samples. Insets show the square wave voltammograms of the PBI/MWCNT-modified CNF-based printed electrode for sea water samples containing different concentration of AMX with supporting electrolyte of 0.1 M Na_2SO_4 solution (pH 7).

References

1 C. Chen, X. Bu, Q. Feng, and D. Li, *Polymers*, 2018, **10**, 1000.
2 M. Tominaga, K. Kuwahara, M. Tsushida, and K. Shida, *RSC Advances,* 2020, **10**, 22120–22125.
3 A. D. Becke, *J. Chem. Phys.*, 1993, **98**, 5648–5652.
4 A. D. McLean and G. S. Chandler, *J. Chem. Phys.*, 2008, **72**, 5639–5648.
5 R. Krishnan, J. S. Binkley, R. Seeger, and J. A. Pople, *J. Chem. Phys.*, 1980, **72**, 650–654.
6 M. J. Frisch *et al.*, *Gaussian 09, Revision A.02*. Wallingford CT: Gaussian, Inc., 2016.
7 R. Gholami and M. Solimannejad, *Struct. Chem.*, 2023, **34**, 577–584.
8 H. Juwono, A. F. Imron, N. I. Oktavianti, A. L. Ivansyah, and Y. Kusumawati, *Monatshefte Für Chem. - Chem. Mon.*, 2022, **153**.
9 A. O. Osikoya, F. Opoku, and P. P. Govender, *Chem. Phys. Lett.*, 2021, **764**, 138278.
10 M. Ding, D. C. Sorescu, and A. Star, *J. Am. Chem. Soc.*, 2013, **135**, 9015–9022.
11 A.J. Bard and L.R. Faulkner, *Electrochemical methods: fundamentals and applications*, John Wiley & Sons, 2001, pp. 569–572.
12 M. Tominaga, S. Sakamoto, and H. Yamaguchi, *J. Phys. Chem. C,* 2012, **116**, 9498–9506.